processes

MDPI

Article

Tertiary Treatment of Pulp Industry Effluents Using Activated Biochar Derived from Biological Sludge Within a Circular Economy Framework

Antonio Machado Netto [1], Marília Christian Gomes Morais Nascimento [2], Leonardo Souza de Caux [2], Marcela de Oliveira Brahim Cortez [1], José Pedro Rodrigues Ferreira [1], Keivison Almeida Monteiro [3] and Renata Pereira Lopes Moreira [1,*]

[1] Department of Chemistry, Universidade Federal de Viçosa (UFV), Av. Peter Henry Rolfs, s/n, University Campus, Viçosa 36570-900, MG, Brazil; antonio.netto@ufv.br (A.M.N.); jose.p.ferreira@ufv.br (J.P.R.F.)
[2] Celulose Nipo-Brasileira S. A. (CENIBRA), Rodovia Br 381 Km 172, Distrito Perpétuo Socorro, Belo Oriente 35196-972, MG, Brazil; marilia.morais@cenibra.com.br (M.C.G.M.N.); leonardo.caux@cenibra.com.br (L.S.d.C.)
[3] Instituto Acadêmico de Ciências e Tecnologias (IACT), BR 153 Fazenda Barreiro do Meio, UEG Central Campus, Universidade Estadual de Goiás (UEG), Anápolis 75132-903, GO, Brazil; keivison.monteiro@ueg.br
* Correspondence: renata.plopes@ufv.br; Tel.: +55-31-98841-1861

Abstract: The application of circular economy principles to the sustainable management of waste from the pulp industry presents significant environmental challenges. In this context, using biological sludge as a raw material for producing activated biochar (BC) emerges as a promising and sustainable alternative. This study evaluated the valorization of biological sludge through the synthesis of activated BC for the removal of color, chemical oxygen demand (COD), and conductivity from the industry's effluent. BC was produced using chemical activation with phosphoric acid (H_3PO_4) and potassium hydroxide (KOH), followed by pyrolysis at 500 °C and 450 °C, respectively. A central composite rotational design (CCRD) was applied to optimize the process. The optimized BCs were characterized by proximate analysis, FTIR, BET surface area, higher heating value (HHV), and SEM. Adsorption assays showed that H_3PO_4-activated BC achieved removal efficiencies of 52.2% for color, 23.9% for COD, and 46.2% for conductivity at a dosage of 5 g L^{-1}. Conversely, KOH-activated BC did not perform effectively. The results highlight the influence of activation and pyrolysis on BC properties and confirm the potential of this approach for the tertiary treatment of industrial effluents, contributing to waste valorization and environmental sustainability.

Keywords: adsorption; pyrolysis; sustainability; industrial effluent; biomass; waste management; circular economy

check for updates

Academic Editor: María Cristina Area

Received: 22 April 2025
Revised: 17 May 2025
Accepted: 20 May 2025
Published: 23 May 2025

Citation: Netto, A.M.; Nascimento, M.C.G.M.; de Caux, L.S.; Cortez, M.d.O.B.; Ferreira, J.P.R.; Monteiro, K.A.; Moreira, R.P.L. Tertiary Treatment of Pulp Industry Effluents Using Activated Biochar Derived from Biological Sludge Within a Circular Economy Framework. *Processes* **2025**, *13*, 1647. https://doi.org/10.3390/pr13061647

Copyright: © 2025 by the authors. Licensee MDPI, Basel, Switzerland. This article is an open access article distributed under the terms and conditions of the Creative Commons Attribution (CC BY) license (https://creativecommons.org/licenses/by/4.0/).

1. Introduction

The continuous growth of the agricultural and industrial sectors underscores the rising need for effective waste management and the adoption of circular economy principles. In this context, the pulp industry stands out as one of the most prominent on the global stage, requiring the management of large volumes of biomass throughout various processing stages, from plantation to waste management [1]. In addition to its main products, the pulp industry also generates characteristic by-products such as grits and dregs, ashes, and biological sludge (BS), originating from the causticizing process, boiler combustion, and effluent treatment, respectively. If not recovered, these by-products are classified as waste

and must be properly managed, posing both environmental and economic challenges [2]. Furthermore, this sector is notable for its high water consumption and the consequent generation of effluents [3].

The effluent from the pulp industry has a complex composition of organic and inorganic pollutants, varying according to the raw materials used and the methods applied in the production process [4]. Untreated, these effluents exhibit high levels of organic matter and suspended solids, with chemical oxygen demand (COD) levels exceeding 1000 mg L^{-1}, along with the presence of sulfites and sulfides [5]. The pulp production process generates highly toxic components, including chlorinated lignin degradation products such as chlorolignins, chlorophenols, and chloroaliphatic compounds [5]. Lignin, a major component of wood, constitutes a significant portion of the effluent, contributing to elevated COD levels and imparting a dark coloration [6]. In this regard, the presence of toxic components and dark coloration can lead to environmental impacts, prompting frequent changes in environmental regulations that are becoming progressively stricter regarding discharge parameters for these wastewater streams.

Biological sludge (BS), generated from the primary and secondary treatment of effluent at pulp mills, has been the focus of numerous works and applications aimed at enhancing its management and utilization. Energy recovery from this biomass has been explored as a viable valorization alternative, with a focus on combustion for heat and electricity generation [7,8]. However, factors such as high moisture content and the presence of inorganic materials in BS lead to low energy efficiency, as well as operational challenges, such as the development of corrosion in equipment [8,9].

Thus, pyrolysis stands out as a satisfactory treatment option due to its ability to convert biomass into three fractions as follows: solid (biochar), oily (bio-oil), and gaseous (biogas), which can be reused for applications in various fields [10,11]. Furthermore, this process avoids certain technical issues, such as the formation of scale, which is common in combustion systems, as it occurs at lower temperatures (300 to 600 °C) and in an inert atmosphere [2].

The solid fraction, known as activated biochar (BC), is a material with a high carbon content, characterized by a surface rich in functional groups, high porosity, charge, and a large surface area. These properties can be enhanced through a chemical activation process, optimizing its applications [12]. This material can be employed in the tertiary treatment of effluents generated by the industry itself, acting as an adsorbent in contaminant removal processes. This strategy is considered a promising approach among various treatment techniques aimed at improving effluent quality [13].

The characteristics of BC are directly related to the composition of the raw material, the activating agent, and the pyrolysis conditions employed. These factors distinctly influence the material's ability to remove pollutants [14]. The most used activating agents in chemical activation are phosphoric acid (H_3PO_4), sodium hydroxide (NaOH), and potassium hydroxide (KOH) [15]. In this regard, the chemical properties of these agents influence the final characteristics of BC, depending on the interactions established with the biomass. These factors impact the material's ability to remove pollutants. According to Ahmed et al. [16], alkaline modification, in comparison to acid modification, typically enhances the surface aromaticity and increases the nitrogen-to-carbon ratio, while decreasing the oxygen-to-carbon ratio. Moreover, activation with H_3PO_4 favors an increase in pyrolysis yield, as it protects the pore structure of biochar, preventing the excessive burning of the carbon structure [13].

Thus, this work aims to support the pulp industry by aligning with circular economy principles and addressing environmental requirements. To achieve this, the valorization of biological sludge through its conversion into activated biochar is proposed, to be ap-

plied as an adsorbent in advanced treatment processes for the removal of contaminants from industrial effluent. Therefore, this work aims to optimize the synthesis of activated biochar from the biological sludge of the pulp industry with different activating agents, using the Response Surface Methodology (RSM) through a Central Composite Rotational Design (CCRD), and to apply the optimized biochars in the removal of color, COD, and effluent conductivity.

This work explores a sustainable approach by repurposing industrial waste from secondary effluent treatment for use in tertiary treatment within the same facility. This closed-loop strategy aligns with the principles of the circular economy, demonstrating a practical model for on-site waste valorization that supports both environmental sustainability and economic benefits for the industry.

2. Materials and Methods

2.1. Reagents and Solutions

The analytical-grade reagents used were hydrochloric acid 37% (CAS 7947-01-0, Fmaia Indústria e Comércio Ltd., Cotia, São Paulo, Brazil), phosphoric acid 85% (CAS 7664-38-2, NEON Comercial Ltd., Suzano, São Paulo, Brazil), potassium hydroxide 85.5% (CAS 1310-58-3, NEON Comercial Ltd., Suzano, São Paulo, Brazil), sodium hydroxide 98.93% (CAS 1310-73-2, NEON Comercial Ltd., Suzano, São Paulo, Brazil), humic acid 99,8% (CAS 1415-93-6, Sigma Aldrich, Saint Louis, MO, USA), and commercial powdered activated carbon (CAS 7440-44-0, Nuclear Comércio e Representações Ltd., Diadema, São Paulo, Brazil). Deionized water, obtained through the ion exchange process, was used for solution preparation.

2.2. Biomass and Industrial Effluent Acquisition

The biomass and effluent were obtained from the Biological Treatment Station (BTS) of a pulp-producing company in the state of Minas Gerais, Brazil. The BS was collected in plastic sampling bags with a volume of 20 L after biological treatment, polymer dosing, and pressing, resulting in a moisture content of 87.16%. The material was stored under refrigeration (4 °C) to prevent the decomposition of organic matter and the proliferation of microorganisms.

The industrial effluent was collected in plastic sampling bottles with a volume of 3 L after secondary treatment and was used immediately to preserve its characteristics and prevent alterations in its composition.

2.3. Synthesis of Biochars

For the synthesis of BC, the Response Surface Methodology (RSM) was applied using a Central Composite Rotational Design (CCRD) with Minitab Student software version 17 (Minitab LLC, State College, PA, USA). The input variables evaluated were (1) the impregnation ratio (mass of activating agent per mass of biomass) and (2) the residence time in the reactor, with the experimental setup and the values used for these variables shown in Figure S1. The response variable used for optimization was iodine number, a commonly used assay to assess the adsorption behavior of BC. The experimental design is shown in Table S1, containing 4 factorial points, 4 axial points, and 5 central repetitions.

Chemical activation was carried out using phosphoric acid (H_3PO_4) and potassium hydroxide (KOH) at mass ratios (mass of activator/mass of dried BS), producing acid-activated biochar (BA) and base-activated biochar (BB), respectively. The mixture was then dried in an oven at 105 °C for 24 h. The material was pyrolyzed in a pyrolysis reactor (Figure S2) equipped with a muffle furnace and a thermocouple at temperatures of 500 °C

and 450 °C for BA and BB, respectively, with an average heating rate of 20 °C min^{-1} and a nitrogen flow rate of 13.5 L h^{-1}.

The bio-oil (BO), composed of condensable gases, was collected and its yield was analyzed. The quantification of biogas (BG) was performed through mass balance. After the reactor cooled down, the biochar (BC) was recovered and sieved to a 32-mesh size.

The BCs were washed in two stages. First, they were placed in contact with a NaOH solution (0.5 mol L^{-1}) and a HCl solution (1.5 mol L^{-1}) for 30 min for BAs and BBs, respectively. Then, they were washed with distilled water for 15 min to achieve a near neutral pH and remove residual ashes formed during pyrolysis, as described by Reddy et al. [17]. Subsequently, the BCs were dried in an oven at 105 °C for 24 h.

The yield of the pyrolysis process was calculated using Equation (1).

$$Y\ (\%) = \left(\frac{m_P}{m_T}\right) * 100 \quad (1)$$

where Y is the yield (%); m_P is the mass of the produced material (g); and m_T is the initial mass before pyrolysis (g).

2.4. Characterization of the Materials

The iodine number quantification was used as the response to optimize the biochar synthesis, following the experimental design CCRD (Table S1). This parameter was measured according to the NBR 12073 standard [18]. The response surface was generated using Minitab Student software. After defining the synthesis parameters for the optimized biochars (BAO and BBO), the characterization of these materials and the biological sludge was carried out.

The biological sludge, optimized H_3PO_4-activated biochar (BAO), and optimized KOH-activated biochar (BBO) were first characterized by determining their fixed carbon, moisture, ashes, and volatile compounds [19].

The contents of C, H, N, and S were determined by elemental analysis [20], using the LECO—TruSpec Micro equipment (LECO Corporation, St. Joseph, MI, USA), and the estimation of oxygen content was obtained by subtracting the sum of the contents of these elements from 100%.

The higher heating value (HHV) was determined by calorimetry [21] using a bomb calorimeter (C200, IKA, Breisgau, Germany). The determination of the total organic carbon (TOC) was performed using a TOC analyzer (TOC-L CPH ver. 1.04, Shimadzu Corporation, Kyoto, Japan).

Characterization by Fourier Transform Infrared Spectroscopy (FTIR) was carried out using the attenuated total reflectance technique, using the spectrum (Pike GladiATR, IRPrestige21, Shimadzu Corporation, Japan) and transmittance scans in the range from 450 to 4000 cm^{-1}.

BAO and BBO were also characterized by specific surface area (SBET), determined through nitrogen adsorption and desorption isotherms, performed in a BET analyzer (NOVA 600, Anton Paar, Graz, Austria), following the gasification of the sample at 353 K for 4 h. From the SBET, the pore diameter was calculated using the Functional Density Theory (FDT) method.

Scanning Electron Microscopy (SEM) analysis was performed using a FIB—Quanta FEG 3D FEI microscope (FEI Company, Hillsboro, OR, USA), which was coupled with Energy Dispersive Spectroscopy (EDS) for inorganic analysis.

X-ray diffraction (XRD) analysis was performed using a diffractometer (D8 Discover, Bruker Corporation, Karlsruhe, Germany) equipped with a copper anode and a Göbel mirror.

Thermogravimetric analyses (TGA) were performed using a thermogravimetric analyzer (DTG-60H, Shimadzu Corporation, Japan), with a heating rate of 10 °C min^{-1}, s temperature range from 20 to 840 °C, and an inert N_2 atmosphere with a flow rate of 50 mL min^{-1}.

The point of zero charge $pH_{(PZC)}$ was determined using the method described by De Souza et al. [22].

The metal analysis of the effluent was performed using inductively coupled plasma optical emission spectrometry (ICP-OES) with an iCAP PRO spectrometer (Thermo Scientific, Waltham, MA USA), following method 6010D [23].

2.5. Adsorption Assays

In the adsorption assay, the BCs (50 mg) were exposed to the effluent (50 mL) in an orbital shaker at 170 rpm, with varying contact times for the kinetic study and a fixed equilibrium time of 90 min for the isothermal study, maintaining a room temperature (~25 °C). After the shaking period, the solution was filtered through a 45 µm membrane, and the effluent color after adsorption was quantified using UV-Vis spectroscopy, following the single-wavelength spectrophotometric method 2120 C [24].

The adsorption capacity was determined according to Equation (2).

$$q = \frac{C_{in} - C_{out}}{m_{ad}} \tag{2}$$

where q is the adsorption capacity (CU g^{-1}), C_{in} is the initial color of the effluent (CU), C_{out} is the final color of the effluent (CU), and m_{ad} is the mass of the adsorbent (g).

Kinetic studies were conducted using an effluent volume of 50 mL and a 1.00 g L^{-1} dosage of adsorbent material, with samples collected at intervals ranging from 15 to 180 min. The pseudo-first-order kinetic model, Equation (3), [25], and the pseudo-second-order kinetic model, Equation (4), [26], were fitted to the experimental data.

$$q_t = q_e\left[1 - e^{-k_1 t}\right] \tag{3}$$

$$q_t = \frac{k_2\, q_e^2\, t}{1 + k_2\, q_e\, t} \tag{4}$$

where q_e and q_t are the amounts adsorbed per gram of adsorbent at equilibrium and at time t (min), respectively, in CU g^{-1}; k_1 is the pseudo-first-order adsorption rate constant (min^{-1}); and k_2 is the pseudo-second-order adsorption rate constant (g CU^{-1} min^{-1}).

The adsorption isotherms were determined by evaluating color removal at adsorbent doses ranging from 1.0 to 5.0 g L^{-1} at room temperature (~25 °C). The Langmuir [27] and Freundlich [28] models were fitted to the experimental data, according to Equations (5) and (6), respectively.

$$q_e = \frac{q_{max}\, K_L\, C_e}{1 + K_L\, C_e} \tag{5}$$

$$q_e = K_F C_e^{\frac{1}{n}} \tag{6}$$

where q_{max} is the maximum adsorption capacity (CU g^{-1}); K_L is the adsorbate/adsorbent interaction constant (L g^{-1}); C_e is the adsorbent concentration (g L^{-1}); K_F is the Freundlich adsorption capacity constant ($CU^{1-(1/n)}$ g^{-2} $L^{1/n}$); and $1/n$ is the constant related to the surface heterogeneity.

Additionally, the data for COD and conductivity were collected to determine the removal of these parameters at these concentrations, using the colorimetric method 5220 D [29] and the conductimetric method 2510 B [30], respectively.

Furthermore, the COD removal potential of the optimized biochar was compared with that of commercial activated carbon using a 50 mg L^{-1} humic acid solution. The adsorption process was conducted over a period of 1440 min, at a temperature of 25 °C, and with an adsorbent concentration of 1.00 g L^{-1}. COD was determined using the colorimetric method 5220 D [29].

2.6. Statistical Analysis

To evaluate the statistical influence of the input variables on the iodine number during optimization, as well as between samples in the kinetics and isotherm experiments of the biochar, a two-way analysis of variance (ANOVA) with repetition ($p \leq 0.05$) was used. In addition, the kinetic and adsorption isotherm models were fitted to the experimental data, and the selection of the most suitable model was based on the coefficient of determination (R^2), the adjusted coefficient of determination (R^2adj), and the two-way ANOVA with repetition.

3. Results and Discussion

3.1. Optimization of Biochar Synthesis

The yields obtained from the pyrolysis and total production of BCs, derived from biomass activated with H_3PO_4 and KOH, including the thirteen biochars defined by CCRD, BAO, and BBO, are presented in Table 1. During biochar production, mass losses occurred primarily during the pyrolysis stage, due to the release of condensable volatile compounds (bio-oil), non-condensable compounds (biogas), and the removal of ash during washing.

Table 1. Yield (%) of biochar (BC), bio-oil (BO), and biogas (BG), and iodine number of BAs (H_3PO_4-activated biochar) and BBs (KOH-activated biochar).

Code	Final Pyrolysis Composition (%)			Final Yield *	Iodine Number
	BC	BO	BG	(%)	(mg I_2 g^{-1})
BA1	67.76	0.64	31.6	27.53	518.4
BA2	59.58	3.13	37.29	40.96	475.43
BA3	65.14	2.04	32.82	42.87	537.82
BA4	70.94	0.5	28.56	35.62	557.84
BA5	56.06	4.95	38.99	44.7	441.28
BA6	63.45	3.75	32.8	33.32	475.18
BA7	60.12	1.29	38.59	41.89	536.75
BA8	60.92	1.83	37.25	37.99	534.8
BA9	58.07	1.78	40.15	40.98	375.09
BA10	61.32	5.02	33.66	36.82	528.43
BA11	61.6	1.86	36.53	37.24	495.33
BA12	65.27	2.89	31.84	40.67	553.13
BA13	61.67	3.27	35.07	40.13	519.31
BAO	59.94	1.95	38.11	56.44	510.66
Average BAs	62.27	2.49	35.23	39.8	
BB1	81.18	0.24	18.58	15.95	274.86
BB2	63.8	0.14	36.05	29.47	351.74
BB3	69.06	1.33	29.61	23.13	296.83
BB4	79.48	0.37	20.15	19.11	266.14
BB5	61.32	0.15	38.53	25.11	295.76
BB6	68.79	1.08	30.13	18.94	245

Table 1. *Cont.*

Code	Final Pyrolysis Composition (%)			Final Yield *	Iodine Number
	BC	BO	BG	(%)	(mg I_2 g^{-1})
BB7	64.72	0.34	34.94	26.04	324.51
BB8	69.02	1.48	29.51	23.87	282.64
BB9	67.15	1.08	31.77	24.76	262.87
BB10	67.75	0.84	31.41	24.32	270.47
BB11	68.87	2.03	29.11	21.79	287.68
BB12	69.78	1.29	28.94	24.65	270.88
BB13	67.71	2.28	30.01	22.07	296.46
BBO	61.58	1.43	36.99	29.01	328.44
Average BBs	68.59	1.01	30.41	23.44	

* Total process yield, related to BC mass production after washing.

The overall yield of the process for BB (KOH-activated biochar) and BA (H_3PO_4-activated biochar) is consistent with values reported in the literature. Thivaly et al. [31] reported yields ranging from 14.23 to 26.25% for biochars obtained from coconut waste, activated with KOH and pyrolyzed at temperatures between 400 and 500 °C. These values were lower than those reported by Chen et al. [32], who produced biochars from wood chips activated with H_3PO_4. According to the authors, yields between 24.8 and 42.3% by mass were achieved. This trend is expected, as alkaline activators induce more intense degradation of the carbonaceous structure, leading to lower yields. On the other hand, acid activators facilitate a more controlled modification of the biomass, promoting the formation of well-defined pores while preserving the integrity of the carbon structure [33].

The iodine number (Table 1) was selected as the response for optimization because it can predict adsorption efficiency, as it provides information related to the distribution of micropores present in the biochars [32]. These values were used in the ANOVA of BA and BB, and the results are shown in Tables S2 and S3, respectively. The analysis of BB and BA indicates that the quadratic model is statistically significant ($\alpha < 0.05$). However, for BA, only the pyrolysis time was significant, while for BB, the impregnation ratio was the only factor with significance.

The determination coefficients R^2 and R^2adj demonstrated a strong correlation between the predicted and observed values for the iodine number response variable. Additionally, the lack-of-fit test was not significant, indicating no statistical evidence of model inadequacy in describing the data. Therefore, the relationships between the input variables ((A) pyrolysis time; (B) impregnation ratio) and the output variable (iodine number) for BA and BB are represented by Equations (7) and (8), respectively. These models were then used to optimize the process parameters and guide the production of the optimized biochars (BAO and BBO).

$$\text{Iodine number} = -611 + 38.17 * A + 285 * B - 0.3606 * A^2 - 216 * B^2 + 1.42 * A * B \quad (7)$$

$$\text{Iodine number} = 378 + 5.82 * A - 554 * B - 0.0618 * A^2 + 268.1 * B^2 + 0.85 * A * B \quad (8)$$

The variations in iodine number as a function of pyrolysis time for BA and impregnation ratio for BB, both significant variables, are shown in Figure 1 and Figure S3, along with their respective response surfaces. For BA (Figure 1a), the pyrolysis time follows a parabolic trend with a downward concavity, reaching its maximum at 54 min. In the case of BB (Figure 1b), the impregnation ratio also exhibits a parabolic trend but with an upward concavity, with higher values observed at the extremes, particularly at a ratio of 0.4, which stood out as the most prominent. As for the other independent variables, their

lack of statistical significance indicates that they do not have a relevant influence on the optimization of biochar production.

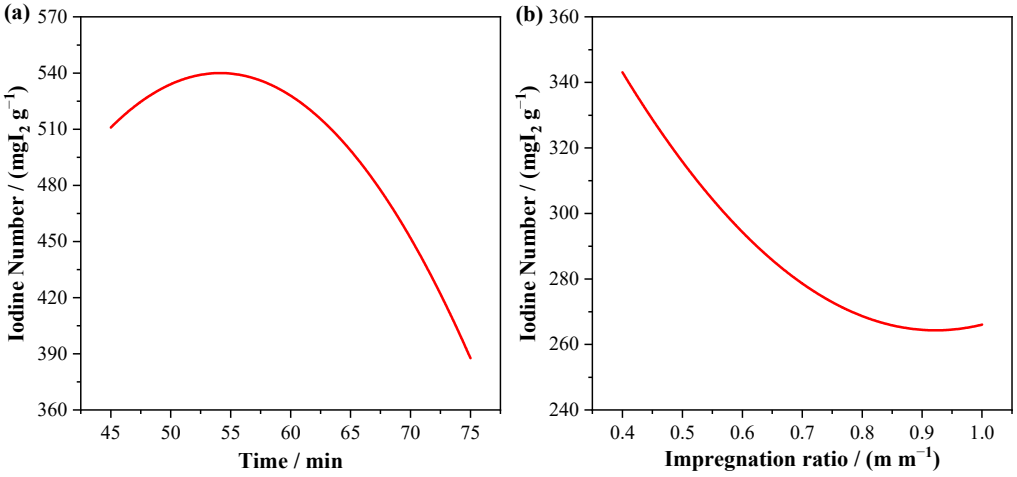


Figure 1. Effect plots relating (**a**) time and (**b**) impregnation ratio with the iodine number responses found for BA (H_3PO_4-activated biochar) and BB (KOH-activated biochar), respectively.

Thus, to produce BAO, a pyrolysis time of 54 min was selected, with the impregnation ratio set to 0.40 m m^{-1} to reduce reagent consumption. For BBO, the impregnation ratio was also set to 0.40 m m^{-1}, while the pyrolysis time was adjusted to 45 min to minimize the process' energy demand.

Table 2 presents the predicted and observed results, along with the relative errors for the iodine number test of BAO and BBO. The low relative errors indicate a strong agreement between experimental and predicted values, reinforcing the reliability of the optimization process.

Table 2. Iodine number of the optimized biochars, in mg I_2 g^{-1}, predicted and observed.

Code	Predicted	Observed	Relative Error (%)
BAO *	508.69	510.66	0.39%
BBO **	351.02	328.44	6.43%

* BAO (optimized H_3PO_4 − activated biochar), and ** BBO (optimized KOH − activated biochar).

3.2. Characterization of Materials

The results of the immediate and elemental analyses, TOC, HHV, S_{BET}, average pore diameter, and EDS are shown in Table 3. The fixed carbon content nearly doubled in BAO and BBO compared to the sludge, indicating a significant improvement. These results suggest that BAO and BBO may exhibit greater efficacy in contaminant removal in adsorption applications [34]. An increase in ash content is also observed, which may be related to the decomposition of the organic fraction and its release through volatilization, while inorganic components are retained [35]. Furthermore, the decrease in volatile matter content is related to the pyrolysis temperature, with values of 500 and 450 °C for BAO and BBO, respectively. The increase in this parameter promotes a greater reduction in volatile components in the material [35].

The results from the elemental analysis showed that both BAO and BBO exhibited an increase in carbon content and a reduction in hydrogen due to the carbonization process, which facilitates the release of volatile components [36]. The reduction in sulfur content is particularly noteworthy, as it contributes to lowering greenhouse gas emissions when the material is used for energy recovery. Additionally, BAO exhibits a lower H/C ratio compared to BBO, primarily due to the higher pyrolysis temperature, which reduces

the material's aliphatic character [37]. This process attenuates the presence of functional groups containing hydrogen, resulting in a lower proportion of hydrogen relative to carbon. Furthermore, values exceeding 0.60 in the O/C ratio were observed, a parameter related to the decomposition rate and stability of the material, indicating that these materials tend to have a half-life of less than 100 years [38].

Table 3. Results of the proximate analysis, total organic carbon, calorific value of sludge, S_{BET}, and the average pore diameter of sludge, BAO (optimized H_3PO_4 − activated biochar), and BBO (optimized KOH − activated biochar).

Analysis	Characteristics	Sludge	BAO	BBO
Immediate Analysis (m m^{-1})	Moisture (%)	NP *	6.04	3.73
	Volatile Compounds (%)	71.40	27.92	35.16
	Ashes (%)	12.40	30.96	31.03
	Fixed Carbon (%)	16.20	35.08	30.08
Elemental Analysis (m m^{-1})	C (%)	43.01	47.00	49.50
	H (%)	6.43	3.09	4.19
	N (%)	4.65	5.03	3.52
	S (%)	3.09	0.45	0.64
	O (%)	42.82	44.43	42.15
	H/C	1.79	0.79	1.02
	O/C	0.75	0.71	0.64
Total Organic Carbon (m m^{-1})	TOC (%)	41.53	35.82	42.45
Higher Heating Value	HHV (Kcal kg^{-1})	4565.9	4257.1	4469.2
Energy Dispersive Spectroscopy (EDS) of Inorganics (m m^{-1})	Na (%)	NP *	7.61	1.36
	Mg (%)	NP *	2.58	1.56
	Al (%)	NP *	9.33	20.86
	Si (%)	NP *	10.98	22.60
	P (%)	NP *	63.93	26.20
	K (%)	NP *	1.30	18.77
	Ca (%)	NP *	4.26	8.65
SBET	m^2 g^{-1}	NP *	3.34	15.04
Average Pore Diameter	Nm	NP *	5.29	13.94

* NP: not performed.

Regarding the TOC content analysis, it reflects the carbon present in both the fixed carbon and volatile fractions of the biochar. In this context, the TOC levels in the sludge and BBO remained similar, whereas BAO exhibited a reduction in this component. This behavior is attributed to the more intense degradation of organic matter caused by the acidic activation and higher pyrolysis temperature, which enhance the release of carbon-containing volatiles [39]. This finding is supported by the results from the immediate analysis and yield, indicating a lower volatile content in BAO and a higher percentage of bio-oil generated during its production compared to BBO.

The higher heating value (HHV) of BAO and BBO remained similar to that of the sludge, although a slight reduction was observed, with BAO exhibiting a more pronounced decrease than BBO. This behavior is associated with the pyrolysis temperature and the consequent degradation of the carbonaceous structure [40]. Additionally, the HHV of the biochars is comparable to the values reported by Eloy et al. [41] for wood, a widely used fuel source, which recorded a heating value of 4758 kcal kg^{-1}.

Energy-dispersive X-ray spectroscopy (EDS) analysis (Table 3) confirmed the presence of Al, Si, and Ca in the optimized biochars. These elements originate from the sludge itself, as they were not introduced during the production process [11]. The higher phosphorus content in BAO results from activation with H_3PO_4, while the increased potassium content in BBO is attributed to activation with KOH. Additionally, the significant levels of P and K in BAO and BBO highlight their potential for agricultural applications, as these elements are essential for plant growth and metabolic functions in living organisms [42].

The adsorption and desorption isotherms of BAO and BBO can be observed in Figure 2, showing a type IV isotherm behavior [43]. The surface areas of BAO and BBO were 3.34 and 15.04 $m^2\ g^{-1}$, respectively. These results are superior to those reported by Koetlisi and Muchaonyerwa [44], who obtained biochars from sludge with surface areas ranging from 1.6 to 4.2 $m^2\ g^{-1}$. The S_{BET} analysis indicated that, for BAO, 54.6% of the surface area corresponds to the pore volume, while 45.4% is attributed to the external surface. In the case of BBO, these proportions are 14.6% and 85.4%, respectively. Furthermore, the average pore diameters of BAO and BBO were 5.29 and 13.94 nm, respectively, classifying them as mesopores (2 to 50 nm). Similar results were found by Koetlisi and Muchaonyerwa [44] and Yu et al. [45], who obtained biochars from sludge with average pore diameters of 5.06 and 13.44 nm, respectively.

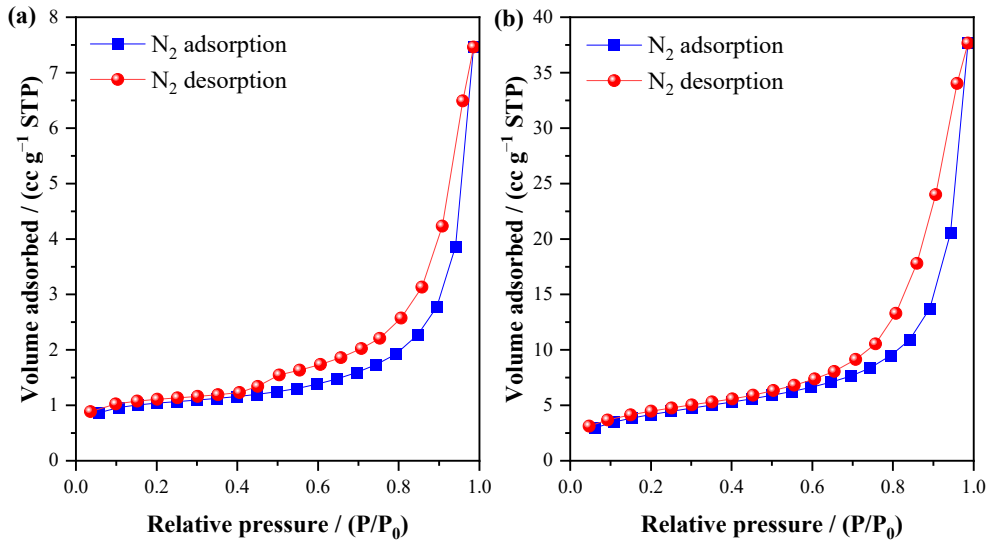


Figure 2. Adsorption and desorption isotherm of N_2 from the optimized biochars. (**a**) BAO (optimized H_3PO_4-activated biochar), and (**b**) BBO (optimized KOH-activated biochar).

Figure 3 shows the morphologies of BAO and BBO, highlighting a rough, layered surface. In BAO, the presence of more pronounced pores is evident, as indicated by the arrows. Ref. [46] also obtained similar results in the synthesis of activated biochars with H_3PO_4 produced from sludge. On the other hand, the BBO image presents a smoother surface with fewer visible pores, consistent with the S_{BET} analysis, which indicates that its surface area is predominantly external.

The FTIR spectra of the sludge, BAO, and BBO are shown in Figure 4. The materials exhibited bands in the region of 1034 cm^{-1}, associated with the stretching of C-O and C-O-C bonds [47,48]. A shift in these bands is observed, along with a reduction in intensity after pyrolysis. This result may be related to the decrease in volatile content in biochars. The band in the region of 1626 cm^{-1}, attributed to the stretching of the C=C bond, suggests the presence of aromatic compounds [49]. The band in the region of 2374 cm^{-1}, related to CO_2, may be associated with its presence in the environment during the analysis [48].

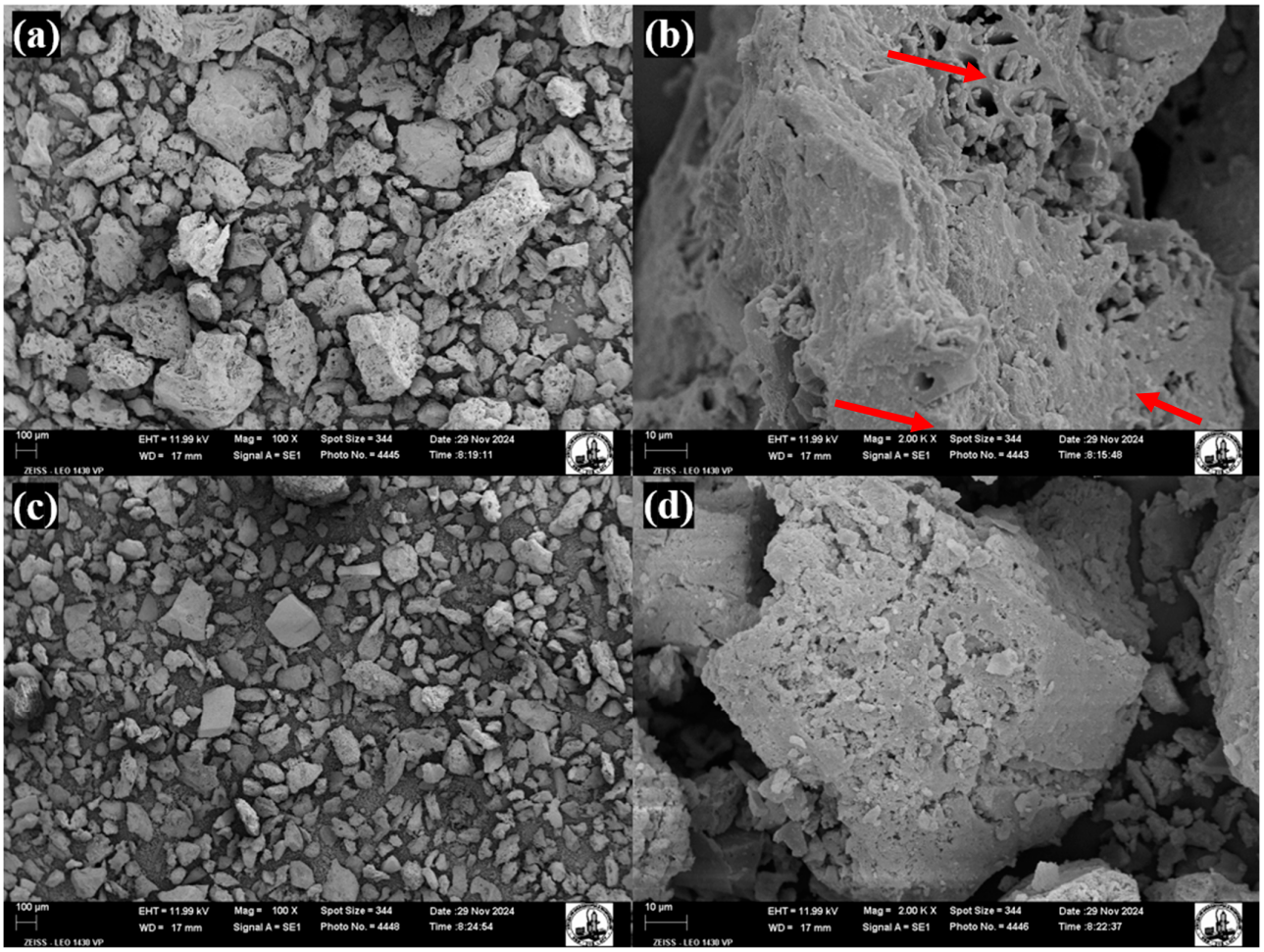


Figure 3. Scanning Electron Microscopy (SEM) images: (**a**,**b**) images of BAO (optimized H_3PO_4-activated biochar) with magnifications of 100× and 2000×, respectively; (**c**,**d**) images of BBO (optimized KOH-activated biochar) with magnifications of 100× and 2000×, respectively.

Additionally, a significant reduction is observed in the band between 3700 and 3000 cm^{-1}, associated with hydroxyl (-OH) groups present in water, alcohols, carboxylic acids, and phenols released during the pyrolysis process [50]. The decrease in the bands between 2990 and 2825 cm^{-1}, associated with aliphatic C-H stretching, indicates the loss of lipid components, as confirmed by the H/C ratio, with a greater reduction observed for BAO [51]. This behavior denotes the elimination of such components in BAO and their preservation in BBO, suggesting the incomplete carbonization of the latter, possibly due to the milder pyrolysis temperature.

The X-ray diffraction (XRD) pattern shown in Figure 5 exhibits peaks at 20.6° and 26.6°, which can be attributed to the presence of silicon dioxide (SiO_2) [52,53]. The peak at 26.6° indicates a high degree of crystallinity of SiO_2, whereas the peak at 20.6° suggests a stronger interaction between silica and the material [53]. A decrease in the peak around 12.1° is also observed with an increase in the pyrolysis temperature, which is a behavior associated with the degradation of partially crystalline cellulose structures present in the biological sludge [54]. Additionally, a peak at 42.5° is detected in the BBO sample, which may be related to the presence of magnesium silicide (Mg_2Si) [55]. The presence of this compound is plausible due to the magnesium content in the biochar, as confirmed by EDS analysis.

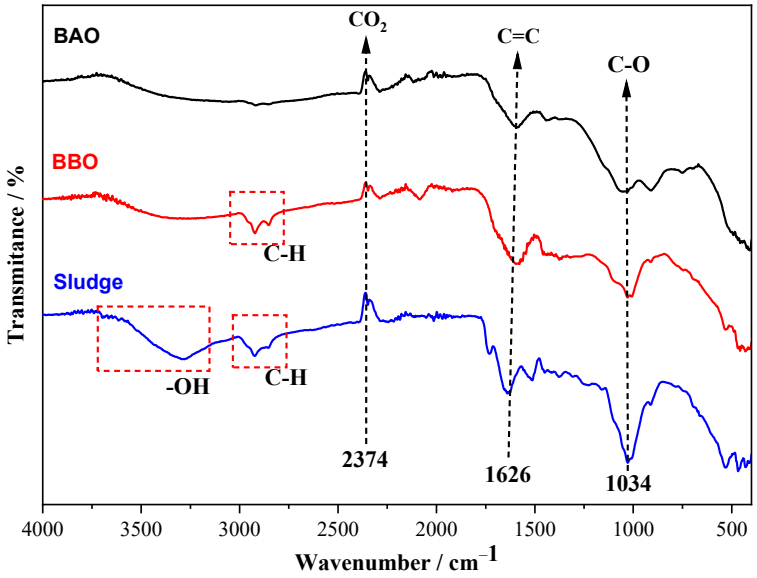


Figure 4. Fourier transform infrared spectrum of the biological sludge, BAO (optimized H_3PO_4-activated biochar), and BBO (optimized KOH-activated biochar).

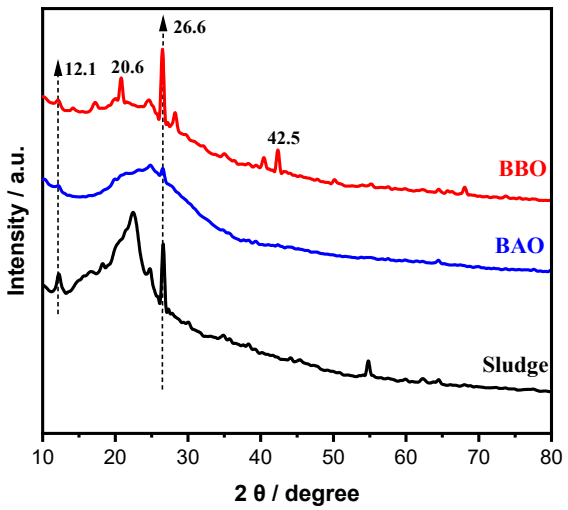


Figure 5. XRD of biological sludge and activated biochars (pyrolysis temperature: BAO (500 °C) and BBO (450 °C)).

The thermogravimetric analysis can be observed in Figure S4, showing the TGA and DTG curves for BAO, BBO, and the sludge. In the temperature range of 25–150 °C, an initial thermal event is observed for all three materials, corresponding to the release of physically adsorbed moisture, a behavior commonly seen in this type of material [56]. Subsequent thermal decomposition processes occur over distinct temperature ranges as follows: hemicelluloses decompose between 250 and 300 °C, cellulose between 300 and 400 °C, and lignin between 400 and 600 °C [57]. The presence of more intense peaks in these temperature ranges can be observed in the thermal analyses of the sludge and BBO (Figure S4b,c), which are related to the presence of non-carbonized organic matter, as confirmed by the FTIR analysis.

The $pH_{(PZC)}$ values for BBO and BAO were 5.73 and 5.15, respectively (Figure S5). This behavior aligns with our expectations, as activation with a basic agent typically leads to an increase in the pH. However, the values did not reach the alkaline range, likely due to the intrinsic properties of the sludge. Guo et al. [58] reported $pH_{(PZC)}$ values ranging from 4.0 to 6.0 for paper mill sludge, reinforcing the acidic nature of this type of material.

Additionally, this characterization allows for predicting the behavior of these materials in relation to the pH of the medium. Below the $pH_{(PZC)}$, the biochar exhibits a positive surface charge, while above this point, it acquires a negative surface charge, which favors the adsorption of compounds with charges opposite to those of the biochar [59].

The metal concentrations in the effluent were determined, and the results are presented in Table 4.

These metals may originate from bioaccumulation in the plants used as raw materials as well as from chemicals employed during the pulp production process [60]. Importantly, none of the detected metals exceed the maximum concentration limits for effluents established by Brazilian environmental regulations [61]. Additionally, toxic metals such as lead, cadmium, chromium, and copper were found at concentrations below the limit of quantification (LOQ) of the analytical method, indicating their minimal presence in the effluent. A notable exception is potassium, which was detected at a significant concentration of 46.5 mg L^{-1}. This value is comparable to the levels reported by Sharma et al. [62], who found potassium concentrations of up to 34.17 mg L^{-1} in effluents from the pulp and paper industries in India.

Table 4. Metal concentrations in the effluent from the pulp industry.

Metals	Concentration (mg L^{-1})	Maximum Permissible Limit (mg L^{-1}) *
Cadmium	<LQ **	0.20
Lead	<LQ **	0.50
Chrome	<LQ **	1.0
Magnesium	2.53 ± 0.05	-
Manganese	0.240 ± 0.0003	1.0
Potassium	46.5 ± 0.05	-
Zinc	0.100 ± 0.0003	5.0
Aluminum (Dissolved)	0.903 ± 0.0003	-
Copper (Dissolved)	<LQ **	1.0
Iron (Dissolved)	1.88 ± 0.05	15.0

* [61]; ** LQ = limit of quantification.

3.3. Adsorption of the Effluent as a Tertiary Treatment

Both materials were evaluated for the removal of color, COD, and conductivity; however, only the results for BAO were satisfactory. The results for BBO, presented in Table S4, show an increase in these parameters over time. This behavior may be attributed to the pyrolysis temperature, as lower temperatures often lead to incomplete biomass decomposition. As a result, partially pyrolyzed materials could be released into the effluent, negatively affecting its quality.

The adsorption kinetics for BAO, as shown in Figure S6, indicate that equilibrium is reached in approximately 90 min. This result is consistent with the findings of Agarwal et al. [63], who reported equilibrium times between 60 and 80 min for color removal from effluents using H_2SO_4-activated biochar derived from wheat straw. Both the pseudo-first-order and pseudo-second-order kinetic models were applied to the experimental data (Table 5), with the pseudo-second-order model providing the best fit. The high R^2 and R^2adj values suggest that the adsorption process is primarily governed by chemisorption [64].

Table 5. Fitting parameters of the kinetic models and determination of the *p*-value according to ANOVA, for effluent adsorption with BAO (optimized H_3PO_4-activated biochar).

Model	q_e (CU g^{-1})	k_1 (min^{-1})	k_2 (g CU^{-1} min^{-1})	R^2	R^2_{adj}	*p*-Value
Pseudo-First-Order	916.124	0.050	-	0.884	0.855	1.82×10^{-5}
Pseudo-Second-Order	1037.448	-	6.516	0.896	0.870	1.46×10^{-5}

p-value = probability of a given statistical measure.

The isotherm results, along with the fittings of the Langmuir and Freundlich models, are shown in Figure 6, and the estimated parameters for both models are presented in Table 6.

Table 6. Isotherm model fitting parameters and *p*-value determination through ANOVA for effluent adsorption using BAO (optimized H_3PO_4-activated biochar).

Model	q_{max} (CU g^{-1})	k_L (L g^{-1})	k_F ($CU^{1-(1/n)}$ g^{-2} $L^{1/n}$)	n	R^2	R^2_{adj}	*p*-Value
Langmuir	75,298.7	0.032	-	-	0.984	0.982	3.88×10^{-8}
Freundlich	-	-	2363.32	1.082	0.982	0.979	5.33×10^{-8}

p-value = probability of a given statistical measure.

The Langmuir model provided the best fit to the data, indicating that adsorption occurs primarily in a monolayer. This suggests a homogeneous distribution of active sites [65,66]. A 52.2% reduction in the color of the tertiary treated effluent was observed at an adsorbent dose of 5.0 g L^{-1}, with the color decreasing from 993.67 CU to 474.69 CU after adsorption. Additionally, based on the maximum adsorption capacity (q_{max}) estimated by the Langmuir model, it is evident that a dose of 7.0 g L^{-1} would provide the highest efficiency for color removal from the effluent.

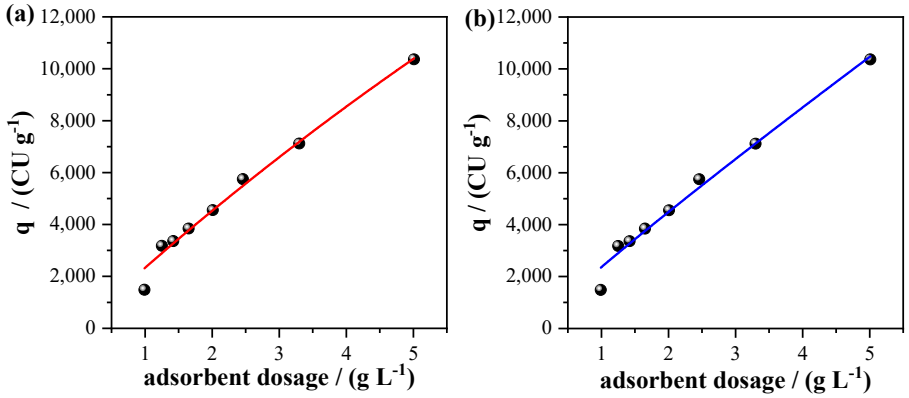


Figure 6. Adsorption isotherms for color removal using BAO (optimized H_3PO_4-activated biochar). Experimental conditions: temperature: ~25 °C; time: 90 min; agitation: ~170 rpm. (**a**) Langmuir model; (**b**) Freundlich model.

Regarding the removal of COD and conductivity, the results obtained can be seen in Figure 7.

The analysis of variance (ANOVA) showed that both responses were significant. Moreover, it is observed that with the adsorbent dose of 5.0 g L^{-1}, there was a reduction of 23.90% in the COD of the treated effluent, decreasing from 374.68 to 285.13 mg O_2 L^{-1} after adsorption. For the same dose of material, conductivity removal was 46.16%, with values decreasing from 2630.0 to 1415.0 µS cm^{-1} after the process. However, it is important to note that, as this is a real effluent, its characteristics may vary depending on the wastewater

generated by the factory. These variations can potentially influence the interaction between the adsorbent and adsorbate, affecting the removal of the three parameters studied.

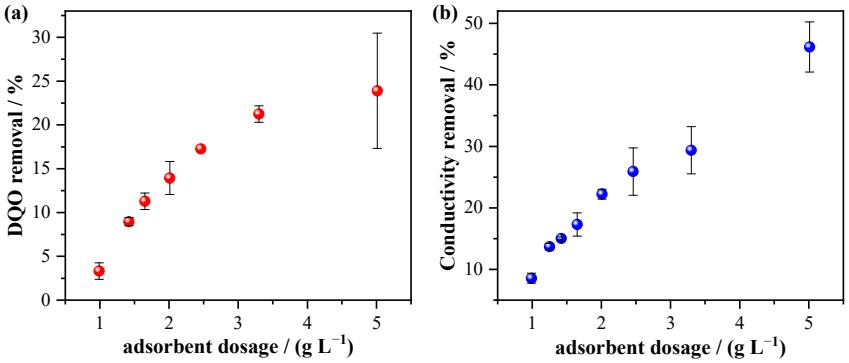


Figure 7. Percentage of COD and conductivity removed in the adsorption with BAO. Experimental conditions: temperature: ~25 °C; time: 90 min; agitation: ~170 rpm. (**a**,**b**) Results of COD and conductivity removal from the effluent, respectively.

A comparison of the performance of BAO with commercial activated carbon was conducted, as shown in Table 7, which presents the COD removal percentages from a humic acid solution using both adsorbents. A real industrial effluent was not used in this analysis due to the variability in its composition over time, which depends on the operational conditions and production stages of the manufacturing plant. Since the adsorption experiments were carried out at different times, using effluent samples collected on separate occasions could have introduced inconsistencies in the results. Therefore, a standard humic acid solution was chosen to ensure experimental reproducibility and enable a reliable performance comparison between the two materials. The results indicate that both adsorbents achieved similar COD removal efficiencies; however, BAO showed a slightly higher removal rate, reinforcing its potential for application in effluent treatment processes.

Table 7. Determination of chemical oxygen demand removal from humic acid solution through adsorption using BAO and commercial activated carbon. Experimental conditions: temperature: ~25 °C; agitation: ~170 rpm; and adsorbent dose: 1.0 g L^{-1}.

Materials	Initial COD (mgO_2 L^{-1})	Final COD (mgO_2 L^{-1})	Removed COD (%)
BAO	80.00	34.98 ± 2.80	56.27
Commercial activated carbon	80.00	39.06 ± 2.21	51.17

BAO before and after humic acid adsorption was analyzed by FTIR, and the results are shown in Figure S7. Band shifts were observed in the range from 1750 to 400 cm^{-1}, which are indicative of humic acid adsorption, confirming the interaction between the material and the adsorbate.

4. Conclusions

The sludge generated by the pulp and paper industry proved to be a promising raw material for producing activated biochar. This study demonstrated the effectiveness of the BC obtained from pulp biological sludge for effluent treatment, highlighting the significant effect of the activation agent on the material's adsorption capacity. The biochar activated with H_3PO_4 showed considerable performance in color, COD, and conductivity removal, achieving removal rates of 52.2%, 23.9%, and 46.2%, respectively, at an adsorbent dose of 5 g L^{-1}, reinforcing its applicability as an effective adsorbent.

In addition to the biochars synthesized for the effluent adsorption process, this work paves the way for future research exploring the energy potential of the by-products generated during pyrolysis, such as bio-oil and biogas. Moreover, further investigations are necessary to evaluate the disposal and post-use applications of the adsorbent material. Potential applications include its combustion for energy recovery or incorporation into soil to enhance water retention, nutrient content, and nitrogen release, thus promoting a more controlled and gradual release of nitrogen. However, additional studies are essential to verify that these uses will not lead to the release of toxic or harmful compounds into the environment.

The findings of this work on the use of biochar (BC) contribute significantly to the valorization of industrial waste, offering a sustainable and environmentally sound solution for wastewater treatment. The adoption of this approach could represent a meaningful advancement for the industrial sector, promoting circular economy principles while minimizing the environmental impacts linked to waste disposal.

Supplementary Materials: The following supporting information can be downloaded at: https://www.mdpi.com/article/10.3390/pr13061647/s1, Figure S1. Experimental setup obtained through the Central Composite Rotational Design; Figure S2: Schematic of the reactor used in the experiments; Figure S3: Response surface plots relating time and impregnation ratio to the iodine number response for (a) BAO (optimized H_3PO_4-activated biochar), and (b) BBO (optimized KOH-activated biochar); Figure S4: Thermogravimetric analysis (TGA) and derivative thermogravimetry (DTG) of the biochars and biological sludge. (a) BAO; (b) BBO; (c) Sludge; Figure S5: Determination of the pH(PCZ) of the optimized biochars (a) BAO (optimized H_3PO_4-activated biochar) and (b) BBO (optimized KOH-activated biochar); Figure S6: Kinetic study of color removal through adsorption with BAO (optimized H_3PO_4-activated biochar). Experimental conditions: temperature: ~25 °C, agitation: ~170 rpm, and adsorbent dose: 1 g L^{-1}; Table S1: Central composite design obtained for the synthesis of biochars produced from the pyrolysis of biological sludge activated with H3PO4 and KOH; Table S2: Analysis of variance (ANOVA) for the determination of the iodine number of the Bas; Table S3: Analysis of variance (ANOVA) for the determination of the iodine number of the BBs; Table S4: Determination of color, COD, and conductivity before and after the adsorption process with BBO.

Author Contributions: A.M.N.: Project administration, Data curation, Formal analysis, Investigation, Methodology, Validation; and Writing—original draft. M.C.G.M.N.: Supervision, Funding acquisition, and Writing—review and editing. L.S.d.C.: Supervision, Funding acquisition, and Writing—review and editing. M.d.O.B.C.: Investigation and Methodology. J.P.R.F.: Conceptualization, Investigation, and Methodology. K.A.M.: Conceptualization, Supervision, and Writing—review and editing. R.P.L.M.: Conceptualization, Supervision, and Writing—review and editing. All authors have read and agreed to the published version of the manuscript.

Funding: This research was funded by Department of Research and Industrial Development of Cellulose Nipo-Brasileira S. A. (CENIBRA).

Data Availability Statement: The original contributions presented in this study are included in the article/Supplementary Materials. Further inquiries can be directed at the corresponding author.

Acknowledgments: The authors would like to thank the Department of Research and Industrial Development of Cellulose Nipo-Brasileira S. A.—CENIBRA; the Department of Chemistry of the Universidade Federal de Viçosa; and the Department of Forest Engineering of the Universidade Federal de Viçosa.

Conflicts of Interest: The authors declare no conflicts of interest. The funders had no role in the design of the study; in the collection, analyses, or interpretation of data; in the writing of the manuscript; or in the decision to publish the results.

Abbreviations

The following abbreviations are used in this manuscript:

BC	Biochar
COD	Chemical Oxygen Demand
CCRD	Central Composite Rotational Design
FTIR	Fourier Transform Infrared Spectroscopy
BET	Brunauer–Emmett–Teller (method for surface area analysis)
HHV	Higher Heating Value
SEM	Scanning Electron Microscopy
BS	Biological Sludge
BO	Bio-oil
BG	Biogas
BA	H_3PO_4-activated Biochar
BB	KOH-activated Biochar
BAO	Optimized H_3PO_4-activated Biochar
BBO	Optimized KOH-activated Biochar
TOC	Total Organic Carbon
S_{BET}	BET Surface Area
EDS	Energy Dispersive Spectroscopy
PZC	Point of Zero Charge
CU	Color Unit
RSM	Response Surface Methodology
ANOVA	Analysis of Variance

References

1. Kataki, R.; Borkotoki, B.; Bora, N.; Maheshwari, S. Valorization of Pulp and Paper Mill Bio-Residues to Biochar for Environmental and Business Sustainability in Totality. *IPPTA Q. J. Indian Pulp Pap. Tech. Assoc.* **2024**, *36*, 179–181.
2. Vilas-Boas, A.C.M.; Tarelho, L.A.C.; Kamali, M.; Hauschild, T.; Pio, D.T.; Jahanianfard, D.; Gomes, A.P.D.; Matos, M.A.A. Biochar from Slow Pyrolysis of Biological Sludge from Wastewater Treatment: Characteristics and Effect as Soil Amendment. *Biofuels Bioprod. Biorefin.* **2021**, *15*, 1054–1072. [CrossRef]
3. Mehmood, K.; Rehman, S.K.U.; Wang, J.; Farooq, F.; Mahmood, Q.; Jadoon, A.M.; Javed, M.F.; Ahmad, I. Treatment of Pulp and Paper Industrial Effluent Using Physicochemical Process for Recycling. *Water* **2019**, *11*, 2393. [CrossRef]
4. Mänttäri, M.; Nyström, M.; Nuortila-Jokinen, J.; Kallioinen, M. Nanofiltration in the Pulp and Paper Industry. In *Nanofiltration*; Schäefer, A.I., Fane, A.G., Eds.; Wiley: Hoboken, NJ, USA, 2021; pp. 599–620. ISBN 978-3-527-34690-5.
5. Shafeeyan, M.S. Application of Photocatalytic and Fenton Processes for the Degradation of Toxic Pollutants from Pulp and Paper Industry Effluents. *Water Resour. Ind.* **2024**, *32*, 100260. [CrossRef]
6. Kamali, M.; Khodaparast, Z. Review on Recent Developments on Pulp and Paper Mill Wastewater Treatment. *Ecotoxicol. Environ. Saf.* **2015**, *114*, 326–342. [CrossRef]
7. Pio, D.T.; Tarelho, L.A.C.; Tavares, A.M.A.; Matos, M.A.A.; Silva, V. Co-Gasification of Refused Derived Fuel and Biomass in a Pilot-Scale Bubbling Fluidized Bed Reactor. *Energy Convers. Manag.* **2020**, *206*, 112476. [CrossRef]
8. Pio, D.T.; Tarelho, L.A.C.; Nunes, T.F.V.; Baptista, M.F.; Matos, M.A.A. Co-Combustion of Residual Forest Biomass and Sludge in a Pilot-Scale Bubbling Fluidized Bed. *J. Clean. Prod.* **2020**, *249*, 119309. [CrossRef]
9. Niu, Y.; Tan, H.; Hui, S. Ash-Related Issues during Biomass Combustion: Alkali-Induced Slagging, Silicate Melt-Induced Slagging (Ash Fusion), Agglomeration, Corrosion, Ash Utilization, and Related Countermeasures. *Prog. Energy Combust. Sci.* **2016**, *52*, 1–61. [CrossRef]
10. Elalami, D.; Carrere, H.; Monlau, F.; Abdelouahdi, K.; Oukarroum, A.; Barakat, A. Pretreatment and Co-Digestion of Wastewater Sludge for Biogas Production: Recent Research Advances and Trends. *Renew. Sustain. Energy Rev.* **2019**, *114*, 109287. [CrossRef]
11. Ribeiro, M.R.; De Moraes Guimarães, Y.; Silva, I.F.; Almeida, C.A.; Silva, M.S.V.; Nascimento, M.A.; Da Silva, U.P.; Varejão, E.V.; Dos Santos Renato, N.; Teixeira, A.P.D.C.; et al. Synthesis of Value-Added Materials from the Sewage Sludge of Cosmetics Industry Effluent Treatment Plant. *J. Environ. Chem. Eng.* **2021**, *9*, 105367. [CrossRef]
12. Qiu, B.; Shao, Q.; Shi, J.; Yang, C.; Chu, H. Application of Biochar for the Adsorption of Organic Pollutants from Wastewater: Modification Strategies, Mechanisms and Challenges. *Sep. Purif. Technol.* **2022**, *300*, 121925. [CrossRef]

13. Kapatel, D.V.; Rotliwala, Y.C.; Patel, H.J. Co-Pyrolysis Based Activated Bio-Char: Characterization and Its Utilization for Secondary Treated Pulp and Paper Industry Wastewater. *Mater. Today Proc.* **2022**, *57*, 1724–1729. [CrossRef]
14. Li, Z.; Yu, D.; Wang, X.; Liu, X.; Xu, Z.; Wang, Y. A Novel Strategy of Tannery Sludge Disposal—Converting into Biochar and Reusing for Cr(VI) Removal from Tannery Wastewater. *J. Environ. Sci.* **2024**, *138*, 637–649. [CrossRef]
15. Wang, J.; Wang, S. Preparation, Modification and Environmental Application of Biochar: A Review. *J. Clean. Prod.* **2019**, *227*, 1002–1022. [CrossRef]
16. Ahmed, M.B.; Zhou, J.L.; Ngo, H.H.; Guo, W.; Chen, M. Progress in the Preparation and Application of Modified Biochar for Improved Contaminant Removal from Water and Wastewater. *Bioresour. Technol.* **2016**, *214*, 836–851. [CrossRef]
17. Reddy, B.S.; Reddy, N.S.; Nam, S.-Y.; Ahn, H.-J.; Ahn, J.-H. Potassium Hydroxide Activated Carbon Derived from Albumen as an Efficient Sulfur Host for Room Temperature Sodium-Sulfur Batteries. *J. Energy Storage* **2022**, *45*, 103666. [CrossRef]
18. *ABNT NBR 12073*; Carvão Ativado Pulverizado—Determinação Do Número de Iodo—Método de Ensaio. Associação Brasileira de Normas Técnicas: São Paulo, Brasil, 1991.
19. *ASTM D1762−84*; Standard Test Method for Chemical Analysis of Wood Charcoal. ASTM International: West Conshohocken, PA, USA, 2021.
20. *ASTM D5373-21*; Standard Test Methods for Determination of Carbon, Hydrogen and Nitrogen in Analysis Samples of Coal and Carbon in Analysis Samples of Coal and Coke. ASTM International: West Conshohocken, PA, USA, 2021.
21. *ASTM D2015-00*; Standard Test Method for Gross Calorific Value of Coal and Coke by the Adiabatic Bomb Calorimeter. ASTM International: West Conshohocken, PA, USA, 2000.
22. De Souza, N.C.S.; Do Carmo Dias, G.; Puiatti, G.A.; De Oliveira, K.L.A.; Vitorino, T.B.; Silva, T.A.; Moreira, R.P.L. Eco-Friendly Photodegradation of Direct Red 80 Dye Mediated by Biochar Decorated with Cobalt Ferrite. *Int. J. Environ. Sci. Technol.* **2025**, *22*, 4263–4280. [CrossRef]
23. *Standart Methods 6010 D*; Inductively Coupled Plasma Optical Emission Spectrometry (ICP-OES). U.S. EPA: Washington, DC, USA, 2023.
24. *Standart Methods 2120 C*; Spectrophotometric—Single—Wavelength Method. U.S. EPA: Washington, DC, USA, 2023.
25. Lagergren, S. Zur Theorie Der Sogenannten Adsorption Geloster Stoffe. *K. Sven. Vetenskapsakademiens Handlingar* **1898**, *24*, 1–39.
26. Ho, Y.S.; McKay, G. A Kinetic Study of Dye Sorption by Biosorbent Waste Product Pith. *Resour. Conserv. Recycl.* **1999**, *25*, 171–193. [CrossRef]
27. Langmuir, I. The Dissociation of Hyfrogen into Atoms. *J. Am. Chem. Soc.* **1912**, *34*, 860–877. [CrossRef]
28. Freundlich, H. On Adsorption in Solutions. *Z. Phys. Chem.* **1906**, *57*, 385–471.
29. *Standart Methods 5220 D*; Closed Reflux, Colorimetric Method. U.S. EPA: Washington, DC, USA, 2023.
30. *Standart Methods 2510 B*; Conductivity. U.S. EPA: Washington, DC, USA, 2023.
31. Thivaly, D.A.; Setyawan, H.Y.; Yusoff, M.Z.M.; Mohamed, M.S.; Farid, M.A.A. Activated Biochar Production from Young Coconut Waste (Cocos Nucifera) as Bioadsorbent: A Pathway through Artificial Neural Network (ANN) Optimization. *Environ. Monit. Assess.* **2024**, *196*, 962. [CrossRef] [PubMed]
32. Chen, Y.; Zhou, C.; Xing, X.; Chen, L.; Yao, B.; Chao, L.; Zhang, Y.; Wang, J.; Dong, J.; Liu, C.; et al. Interconnected Pyrolysis and Activation with In-Situ H3PO4 Activation of Biochar from Pear Wood Chips in a Pilot Scale Dual Fluidized Bed. *Chem. Eng. J.* **2024**, *495*, 153579. [CrossRef]
33. Gao, Y.; Yue, Q.; Gao, B.; Li, A. Insight into Activated Carbon from Different Kinds of Chemical Activating Agents: A Review. *Sci. Total Environ.* **2020**, *746*, 141094. [CrossRef]
34. Beik, F.; Williams, L.; Brown, T.; Wagland, S.T. Development and Prototype Testing of a Novel Small-Scale Pyrolysis System for the Treatment of Sanitary Sludge. *Energy Convers. Manag.* **2023**, *277*, 116627. [CrossRef]
35. Tarelho, L.A.C.; Hauschild, T.; Vilas-Boas, A.C.M.; Silva, D.F.R.; Matos, M.A.A. Biochar from Pyrolysis of Biological Sludge from Wastewater Treatment. *Energy Rep.* **2020**, *6*, 757–763. [CrossRef]
36. da Luz Corrêa, A.P.; Da Silva, P.M.M.; Gonçalves, M.A.; Bastos, R.R.C.; Da Rocha Filho, G.N.; Da Conceição, L.R.V. Study of the Activity and Stability of Sulfonated Carbon Catalyst from Agroindustrial Waste in Biodiesel Production: Influence of Pyrolysis Temperature on Functionalization. *Arab. J. Chem.* **2023**, *16*, 104964. [CrossRef]
37. Oasmaa, A.; Solantausta, Y.; Arpiainen, V.; Kuoppala, E.; Sipilä, K. Fast Pyrolysis Bio-Oils from Wood and Agricultural Residues. *Energy Fuels* **2010**, *24*, 1380–1388. [CrossRef]
38. Rabichi, I.; Sekkouri, C.; Yaacoubi, F.E.; Ennaciri, K.; Izghri, Z.; Bouzid, T.; El Fels, L.; Baçaoui, A.; Yaacoubi, A. Experimental and Theoretical Investigation of Olive Mill Solid Waste Biochar for Vanillic Acid Adsorption Using DFT/B3LYP Analysis. *Water Air Soil Pollut.* **2024**, *235*, 369. [CrossRef]
39. Almahbashi, N.M.Y.; Kutty, S.R.M.; Ayoub, M.; Noor, A.; Salihi, I.U.; Al-Nini, A.; Jagaba, A.H.; Aldhawi, B.N.S.; Ghaleb, A.A.S. Optimization of Preparation Conditions of Sewage Sludge Based Activated Carbon. *Ain Shams Eng. J.* **2021**, *12*, 1175–1182. [CrossRef]

40. Liu, Y.; Ran, C.; Siyal, A.A.; Song, Y.; Jiang, Z.; Dai, J.; Chtaeva, P.; Fu, J.; Ao, W.; Deng, Z.; et al. Comparative Study for Fluidized Bed Pyrolysis of Textile Dyeing Sludge and Municipal Sewage Sludge. *J. Hazard. Mater.* **2020**, *396*, 122619. [CrossRef] [PubMed]
41. Eloy, E.; Pedrazz, C.; Coldebella, R.; Mangin, T.D.S.; Trevisan, R.; Caron, B.O.; Santos, A.D. Effect of Chemical Constituents on the Energetic and Physical Properties of Wood from Forestry Species. *Ciência Rural.* **2024**, *54*, e20230290.
42. Meina, L.; Qiao, M.; Zhang, Q.; Xu, S.; Wang, D. Study on the Dynamic Adsorption and Recycling of Phosphorus by Fe–Mn Oxide/Mulberry Branch Biochar Composite Adsorbent. *Sci. Rep.* **2024**, *14*, 1235. [CrossRef]
43. Thommes, M.; Kaneko, K.; Neimark, A.V.; Olivier, J.P.; Rodriguez-Reinoso, F.; Rouquerol, J.; Sing, K.S.W. Physisorption of Gases, with Special Reference to the Evaluation of Surface Area and Pore Size Distribution (IUPAC Technical Report). *Pure Appl. Chem.* **2015**, *87*, 1051–1069. [CrossRef]
44. Koetlisi, K.A.; Muchaonyerwa, P. Biochar Types from Latrine Waste and Sewage Sludge Differ in Physico-Chemical Properties and Cadmium Adsorption. *Am. J. Appl. Sci.* **2017**, *14*, 1039–1048. [CrossRef]
45. Yu, Q.; Ye, J.; Liu, G.; Liu, M.; Tang, M.; Li, L. Exploring Electron-Transfer Pathways in Co-Pyrolyzed Waste-Derived Carbocatalyst for Enhanced Peroxydisulfate Activation. *Sep. Purif. Technol.* **2025**, *353*, 128313. [CrossRef]
46. Minaei, S.; Zoroufchi Benis, K.; McPhedran, K.N.; Soltan, J. Adsorption of Sulfamethoxazole and Lincomycin from Single and Binary Aqueous Systems Using Acid-Modified Biochar from Activated Sludge Biomass. *J. Environ. Manag.* **2024**, *358*, 120742. [CrossRef]
47. Li, W.-H.; Yue, Q.-Y.; Gao, B.-Y.; Wang, X.-J.; Qi, Y.-F.; Zhao, Y.-Q.; Li, Y.-J. Preparation of Sludge-Based Activated Carbon Made from Paper Mill Sewage Sludge by Steam Activation for Dye Wastewater Treatment. *Desalination* **2011**, *278*, 179–185. [CrossRef]
48. Xiang, J.; Luo, B.X.; Li, J.M.; Mi, Y.; Tian, B.; Gong, S.J.; Zhou, Y.R.; Ma, T.W. Development of KOH and H3PO4-Modified Composite Biochar from Corn Straw and Activated Sludge for Removing Methylene Blue. *Int. J. Environ. Sci. Technol.* **2023**, *20*, 1673–1688. [CrossRef]
49. Fagbayigbo, B.O.; Opeolu, B.O.; Fatoki, O.S.; Akenga, T.A.; Olatunji, O.S. Removal of PFOA and PFOS from Aqueous Solutions Using Activated Carbon Produced from Vitis Vinifera Leaf Litter. *Environ. Sci. Pollut. Res.* **2017**, *24*, 13107–13120. [CrossRef]
50. Zhou, Q.; Liao, B.; Lin, L.; Qiu, W.; Song, Z. Adsorption of Cu(II) and Cd(II) from Aqueous Solutions by Ferromanganese Binary Oxide–Biochar Composites. *Sci. Total Environ.* **2018**, *615*, 115–122. [CrossRef] [PubMed]
51. Cole, E.J.; Zandvakili, O.R.; Xing, B.; Hashemi, M.; Herbert, S.; Mashayekhi, H.H. Dataset on the Effect of Hardwood Biochar on Soil Gravimetric Moisture Content and Nitrate Dynamics at Different Soil Depths with FTIR Analysis of Fresh and Aged Biochar. *Data Brief* **2019**, *25*, 104073. [CrossRef] [PubMed]
52. Thue, P.S.; Lima, D.R.; Lima, E.C.; Teixeira, R.A.; Dos Reis, G.S.; Dias, S.L.P.; Machado, F.M. Comparative Studies of Physicochemical and Adsorptive Properties of Biochar Materials from Biomass Using Different Zinc Salts as Activating Agents. *J. Environ. Chem. Eng.* **2022**, *10*, 107632. [CrossRef]
53. Yuan, J.-H.; Xu, R.-K.; Zhang, H. The Forms of Alkalis in the Biochar Produced from Crop Residues at Different Temperatures. *Bioresour. Technol.* **2011**, *102*, 3488–3497. [CrossRef]
54. Kim, K.H.; Kim, J.-Y.; Cho, T.-S.; Choi, J.W. Influence of Pyrolysis Temperature on Physicochemical Properties of Biochar Obtained from the Fast Pyrolysis of Pitch Pine (*Pinus rigida*). *Bioresour. Technol.* **2012**, *118*, 158–162. [CrossRef]
55. Saucier, C.; Adebayo, M.A.; Lima, E.C.; Cataluña, R.; Thue, P.S.; Prola, L.D.T.; Puchana-Rosero, M.J.; Machado, F.M.; Pavan, F.A.; Dotto, G.L. Microwave-Assisted Activated Carbon from Cocoa Shell as Adsorbent for Removal of Sodium Diclofenac and Nimesulide from Aqueous Effluents. *J. Hazard. Mater.* **2015**, *289*, 18–27. [CrossRef]
56. Streit, A.F.M.; Collazzo, G.C.; Druzian, S.P.; Verdi, R.S.; Foletto, E.L.; Oliveira, L.F.S.; Dotto, G.L. Adsorption of Ibuprofen, Ketoprofen, and Paracetamol onto Activated Carbon Prepared from Effluent Treatment Plant Sludge of the Beverage Industry. *Chemosphere* **2021**, *262*, 128322. [CrossRef]
57. Zhuang, Z.; Liu, Y.; Wei, W.; Shi, J.; Jin, H. Preparation of Biochar Adsorption Material from Walnut Shell by Supercritical CO2 Pretreatment. *Biochar* **2024**, *6*, 11. [CrossRef]
58. Guo, K.; Gao, B.; Yue, Q.; Xu, X.; Li, R.; Shen, X. Characterization and Performance of a Novel Lignin-Based Flocculant for the Treatment of Dye Wastewater. *Int. Biodeterior. Biodegrad.* **2018**, *133*, 99–107. [CrossRef]
59. Georgin, J.; Franco, D.S.P.; Ramos, C.G.; Piccilli, D.G.A.; Lima, E.C.; Sher, F. A Review of the Antibiotic Ofloxacin: Current Status of Ecotoxicology and Scientific Advances in Its Removal from Aqueous Systems by Adsorption Technology. *Chem. Eng. Res. Des.* **2023**, *193*, 99–120. [CrossRef]
60. Haq, I.; Roy, S.; Kalamdhad, A.S. Characterization of Pulp and Paper Mill Wastewater and Its Toxicity Analysis Using Vigna Radiata. In *Environmental Degradation: Monitoring, Assessment and Treatment Technologies*; Haq, I., Kalamdhad, A.S., Dash, S., Eds.; Springer International Publishing: Cham, Switzerland, 2022; pp. 261–269. ISBN 978-3-030-94147-5.
61. BRASIL. Conselho Nacional do Meio Ambiente (CONAMA). Resolução CONAMA nº 430, de 13 de maio de 2011. Dispõe sobre as condições e padrões de lançamento de efluentes, complementa e altera a Resolução nº 357, de 17 de março de 2005. *Diário Oficial da União*, 16 May 2011.

62. Sharma, P.; Iqbal, H.M.N.; Chandra, R. Evaluation of Pollution Parameters and Toxic Elements in Wastewater of Pulp and Paper Industries in India: A Case Study. *Case Stud. Chem. Environ. Eng.* **2022**, *5*, 100163. [CrossRef]
63. Agarwal, S.; Singh, A.P.; Mathur, S. Removal of COD and Color from Textile Industrial Wastewater Using Wheat Straw Activated Carbon: An Application of Response Surface and Artificial Neural Network Modeling. *Environ. Sci. Pollut. Res.* **2023**, *30*, 41073–41094. [CrossRef] [PubMed]
64. Magesh, N.; Renita, A.A.; Siva, R.; Harirajan, N.; Santhosh, A. Adsorption Behavior of Fluoroquinolone(Ciprofloxacin) Using Zinc Oxide Impregnated Activated Carbon Prepared from Jack Fruit Peel: Kinetics and Isotherm Studies. *Chemosphere* **2022**, *290*, 133227. [CrossRef]
65. Feiyan, W.; Yali, Z.; Siling, L.; Zhiqin, C.; Shanshan, L.; Wenkui, L. Biochar from De-Oiled *Chlorella vulgaris* and Its Adsorption on Antibiotics. *Open Chem.* **2024**, *22*, 20230178. [CrossRef]
66. Zou, M.; Tian, W.; Chu, M.; Gao, H.; Zhang, D. Biochar Composite Derived from Cellulase Hydrolysis Apple Branch for Quinolone Antibiotics Enhanced Removal: Precursor Pyrolysis Performance, Functional Group Introduction and Adsorption Mechanisms. *Environ. Pollut.* **2022**, *313*, 120104. [CrossRef]

Disclaimer/Publisher's Note: The statements, opinions and data contained in all publications are solely those of the individual author(s) and contributor(s) and not of MDPI and/or the editor(s). MDPI and/or the editor(s) disclaim responsibility for any injury to people or property resulting from any ideas, methods, instructions or products referred to in the content.